Simulating the Multipath Channel With a Reverberation Chamber: Application to Bit Error Rate Measurements

Evgeni Genender, *Student Member, IEEE*, Christopher L. Holloway, *Fellow, IEEE*, Kate A. Remley, *Senior Member, IEEE*, John M. Ladbury, Galen Koepke, and Heyno Garbe, *Fellow, IEEE*

***Abstract*—We illustrate the use of the reverberation chamber to simulate fixed wireless propagation environments including effects such as narrowband fading and Doppler spread. These effects have a strong impact on the quality of the wireless channel and the ability of a receiver to decode a digitally modulated signal. Different channel characteristics such as power delay profile and RMS delay spread are varied inside the chamber by incorporating various amounts of absorbing material. In order to illustrate the impact of the chamber configuration on the quality of a wireless communication channel, bit error rate measurements are performed inside the reverberation chamber for different loadings, symbol rates, and paddle speeds; the results are discussed. Measured results acquired inside a chamber are compared with those obtained both in an actual industrial environment and in an office.**

***Index Terms*—Bit error rate (BER), digital modulation, multipath, reverberation chamber, wireless propagation, wireless system.**

I. Introduction

In RECENT years, wireless applications have gained in importance and are now used in many different types of environments, from outdoor urban settings to indoor homes, offices, and industrial plants. Manufacturers of wireless systems want to be able to design and test these devices for use in any type of environment. Thus, it is essential to have a reliable, controllable, and repeatable facility where wireless devices can be tested. In fact, wireless industry groups such as the Cellular Telecommunications Industry Association have formed working groups to investigate the use of reverberation chambers for testing wireless devices, an indication of the impact such work may have. While prior work has demonstrated that the reverberation chamber provides a repeatable environment that can simulate a wide range of multipath environments [1] and [2], in the present work, we present implementation-specific details necessary for the use of an electromagnetic reverberation chamber as such a test facility.

The reverberation chamber is essentially an electrically large metallic box. Inside the chamber a metallic paddle (mode stirrer) is rotated, randomizing the electromagnetic fields inside [3]. The field inside the chamber has been proven to be uniform and isotropic (except for fields closer than $\lambda/2$ to the walls and other metallic objects, where λ is the wavelength), which means that in an ideal reverberation chamber, field measurements will be very similar for any location of objects under test or for antennas inside the chamber. The standard deviation of the mean field throughout the chamber is typically the figure of merit used to assess how well the reverberation chamber performs (see [3]). A small standard deviation of the mean field indicates that there are a sufficient number of modes in the chamber and the paddle is large enough to interact with the modes, resulting in the desired probability densities of the field amplitudes and in statistical spatial uniformity. This required field uniformity also implies polarization balance in the chamber, as discussed in [4]–[6].

The reverberation chamber is popular as an alternative test facility for various electromagnetic measurements. Initially, reverberation chambers were used as high-field amplitude test facilities for electromagnetic interference and electromagnetic compatibility (EMI and EMC), [3]–[5], [7]–[16]. Reverberation chambers are currently used for a wide range of other measurement applications. Applications include but are not limited to, determining 1) radiated immunity of components and large systems; 2) radiated emissions; 3) shielding characterizations of cavities, cables, connectors, and materials; 4) antenna efficiency; 5) probe calibration; 6) characterization of material properties; 7) absorption and heating properties of materials; and 8) biological and biomedical effects.

While most of the research and applications of reverberation chambers have been geared toward EMC/EMI, over the last few years, the reverberation chamber has began to emerge as a tool for wireless communication tests as well. Applications include: radiated power of mobile phones [17]; gain obtained by using diversity antennas in fading environments [18], [19]; antenna efficiency measurements [20]; measurements of multiple-input

Manuscript received July 10, 2009; revised November 25, 2009. The field tests at the oil refinery and the 60-storied office building for this work were supported by the Public Safety Communications Research Laboratory of the Office of Law Enforcement Standards at NIST.

E. Genender was with the Electromagnetics Division, Boulder Laboratories, National Institute of Standards and Technology (NIST), U.S. Department of Commerce, Boulder, CO 80305 USA. He is now with the Institut fuer Grundlagen der Elektrotechnik und Messtechnik, Leibniz University of Hannover, Hannover 30167, Germany.

C. L. Holloway, K. A. Remley, J. M. Ladbury, and G. Koepke are with the Electromagnetics Division, Boulder Laboratories, National Institute of Standards and Technology (NIST), U.S. Department of Commerce, Boulder, CO 80305 USA (e-mail: holloway@boulder.nist.gov).

H. Garbe is with the Institut fuer Grundlagen der Elektrotechnik und Messtechnik, Leibniz University of Hannover, Hannover 30167, Germany.

Color versions of one or more of the figures in this paper are available online at http://ieeexplore.ieee.org.

Digital Object Identifier 10.1109/TEMC.2010.2044578

multiple-output systems [21]; simulated Ricean and Rayleigh multipath environments [1], [25]; simulated environments with clustered power delay profiles (PDPs) [26]; measurements of receiver sensitivity of mobile terminals [27]; bit error rate (BER) measurements [24]; and investigating biological effects of cell-phone base-station RF exposure [28]. Effects like Doppler spread and fading, which are a consequence of a dynamically moving environment, can also be simulated inside the chamber by turning the paddle with different speeds or using it in stepped mode.

Reverberation chambers provide a flexible and repeatable test environment, which may also be more efficient than anechoic chambers for performing certain measurements. For example, antenna performance measurements are often carried out in free space or in an anechoic chamber. Typically, such measurements include positioning the measurement antenna over a large number of orientations, which can require a significant amount of time. In the reverberation chamber, this rotation procedure can be dropped because the fields in the chamber are considered isotropic. In [17], a comparison of radiated power measurements in reverberation and anechoic chambers was performed, and the results were closely correlated.

In [1], it was shown that by varying the chamber and/or antenna characteristics, it is possible to generate a wide range of K-factors. The K-factor is a figure of merit that describes the ratio of direct-path received power to that received via reflections. Reference [1] demonstrated that it is possible to simulate various Rician wireless environments by varying the K-factor. Other research groups have demonstrated a proof of concept of the use of reverberation chambers to simulate different wireless channels [22]–[25]. In this paper, we carry out a detailed study of parameters that can affect the simulated multipath wireless channel, including the effect of chamber loading on the RMS delay spread, the effect of using a realistic measurement bandwidth to find the PDP, and the interaction of the chamber time constant and center frequency on the RMS delay spread.

In order to observe the effectiveness of changing the properties of wireless environments inside the reverberation chamber on modulated-signal transmissions, we perform BER measurements. We show that changing the chamber loading has a significant effect on the BER for simple digitally modulated signals having various data rates. We focus on the common representation of a multipath signal as a series of time-shifted, amplitude-shifted replicas of the transmitted signal [29]. In this model, the multipath channel is characterized as a summation of individual impulse responses at discrete points in time. As we will show, this type of multipath channel can be readily simulated by the reverberation chamber when the paddle is moved slowly (with respect to the data rate) or in a stepped mode. We compare measurements of the PDP carried out in the reverberation chamber with the measurements performed in real multipath environments, including an interior office (low multipath), a 60-storied office building (medium multipath), and the highly reflective environment of an oil refinery. As we demonstrate, the method proposed here works well in noisy environments, as well as those with medium and high multipath. The latter are difficult to test in a free-field environment using other methods.

II. Wireless Environment Characterization

A wireless multipath channel at a fixed location can be modeled by its time-varying, discrete-time impulse response [29]. In this model, multipath reflections are modeled as copies of the transmitted signal that have experienced amplitude and phase shifts. Each modified copy of the transmitted signal arrives at the receiver at a later time. For any fixed location between transmitter and receiver, under time-invariant conditions, the channel will have a linear impulse response $h(t,\tau)$. The output $y(t)$ of this time-varying radio channel at time t can be calculated from

$$y(t) = u(t) * h(t,\tau) = \int_{-\infty}^{\infty} h(t,\tau)u(t-\chi)d\chi \qquad (1)$$

where $u(t)$ is the input signal. Multipath components are accounted for by this representation; where τ is the excess delay corresponding to a given multipath component's arrival time.

The ensemble average of the magnitude squared of the time-varying, discrete-time impulse response is referred to as the PDP and is given by

$$\text{PDP}(t) = \left\langle |h(t,\tau_i)|^2 \right\rangle; \qquad (2)$$

where the ensemble average is over τ. This provides a single time-invariant multipath PDP obtained by averaging many $|h(t,\tau_i)|$. Typically, to develop channel models of real-world multipath environments, the ensemble average is calculated over multiple channel response measurements taken at a number of different locations having similar characteristics. These measurements may also be made at a fixed location, but taken at different times, when objects in the environment such as people and cars may be oriented differently from one time to another. In the reverberation chamber, one common method for obtaining the various amplitude, phase, and time shifts is by moving the paddle in discrete steps. In this way, the PDP is found by averaging individual $|h(t,\tau_i)|$, obtained at fixed paddle positions.

Different types of radio propagation environments produce PDPs having different delay times. Long decay times reflected in the PDP can adversely affect the performance of wireless communication systems. One characteristic of the PDP that has been shown to be particularly important in wireless systems that use digital modulation is the RMS delay spread of the PDP, which is the square root of the second central moment of the PDP given by

$$\tau_{\text{rms}} = \sqrt{\frac{\int_0^\infty (t-\tau_0)^2 \text{PDP}(t)\, dt}{\int_0^\infty \text{PDP}(t)\, dt}} \qquad (3)$$

where τ_0 is the mean delay of the propagation channel, given by

$$\tau_0 = \frac{\int_0^\infty t\ \text{PDP}(t)\, dt}{\int_0^\infty \text{PDP}(t)\, dt}. \qquad (4)$$

The RMS delay spread (τ_{rms}) is often used to characterize a wireless communication environment because it can be related to the BER performance of a channel [31], [32]. In fact, Chuang [31] has shown that, for certain digitally modulated signals, independent of the modulation scheme used, the BER is proportional to the quantity $(\tau_{\text{rms}}/T)^2$, where T is the bit period.

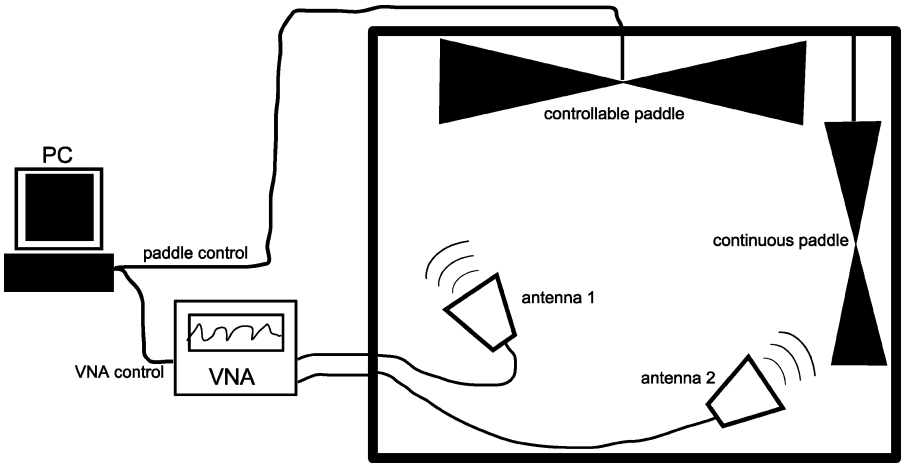

Fig. 1. Measurement setup used to obtain the time-varying, discrete-time impulse response.

The proportionality constant depends on the type of modulation. We next show how the PDP in the reverberation chamber can be controlled and, thus, how the τ_{rms} can be adjusted to give desired values.

III. Controlling the RMS Delay Spread in the Reverberation Chamber

A number of factors go into creating a multipath environment having desired characteristics in the reverberation chamber. These include issues related to creating and measuring the PDP and the RMS delay spread, and methods for proper interpretation of the measured results. We first address issues related to chamber loading to achieve the desired PDP, and then discuss methods for finding the PDP and τ_{rms} from the measured impulse response.

To study the effects of chamber loading on the PDP, we used the measurement setup shown in Fig. 1. The test chamber was the NIST reverberation chamber, having dimensions of 3.05 m $\times$ 4.57 m $\times$ 2.74 m. We placed two dual-ridge horn antennas inside the chamber, connected through a bulkhead by using coaxial cables to a vector network analyzer outside.

In order to control the τ_{rms} of the chamber and thus the PDP, the ring-down duration of the chamber needs to be controlled. Related to ring-down time is the quality factor Q, which is the proportion of energy stored to the energy dissipated per RF cycle

$$Q = \frac{\omega U}{\langle P_d \rangle}; \tag{5}$$

where ω is the radian frequency, U is the energy stored in the cavity, and P_d is the dissipated power. For a given reverberation chamber, the losses resulting from the finite conductivity of cavity walls, the apertures, and the loading caused by the antennas cannot be modified. However, the loading of the chamber can be changed by, for example, putting different numbers of blocks of RF-absorbing material inside the chamber. This reduces the ring-down duration, allowing one to match the τ_{rms} in the chamber to a real radio-propagation environment.

For the large reverberation chamber we used, there is typically no need to increase the ring-down duration, because the unloaded chamber has much larger delay spreads than occur in many real applications (approximately 700 ns at 1 GHz for the unloaded NIST chamber). Metallic structures such as airplanes, metal enclosures, and highly reflective buildings may have longer RMS delay spreads. However, many commerically available reverberation chambers have shorter ring-down times, and therefore, less loading is required to replicate many environments.

In [33], Holloway *et al.* showed that loading a chamber reduces its spatial uniformity. In [33], the chamber was loaded with lossy material, and the average square magnitude of the electric field was measured at random locations in the chamber. The standard deviation over these locations was calculated. The results showed that loading the chamber increased the standard deviation, or in other words, decreased the spatial uniformity. From these results, equations for maximum loading were derived. The maximum loading was expressed in terms of the lowest allowed quality factor Q_{thr} for a given location. It was shown that the actual Q of the chamber must be much greater than the threshold Q_{thr}

$$Q \gg Q_{\mathrm{thr}}. \tag{6}$$

Two equations for calculating Q_{thr} were presented in [33], with a difference between them of a factor of three. In the present paper, the more stringent equation will be used

$$Q_{\mathrm{thr}} = \left(\frac{4\pi}{3}\right)^{2/3} \frac{3V^{1/3}}{2\lambda}; \tag{7}$$

where V is the chamber volume and λ is the wavelength. Note that Q_{thr} indicates only that for a given chamber loading, the spatial uniformity will be significantly disturbed. As a chamber approaches these threshold values, it is necessary to use position, polarization, or frequency stirring to reduce the standard deviation of the ensemble average of the measured fields.

To illustrate the change in Q for different loadings used in this paper, we carried out measurements with different amounts of RF absorber placed in the reverberation chamber. We measured the scattering parameter S_{21} using the vector network analyzer for several paddle positions and determined Q from this quantity,

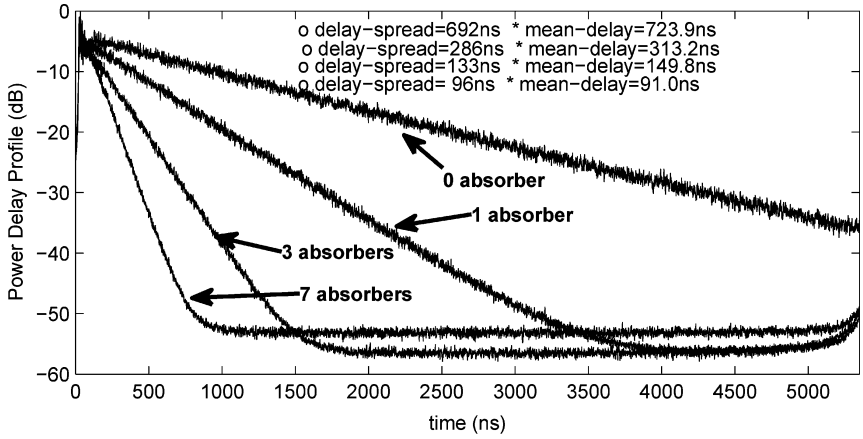

Fig. 2. PDP and RMS delay spread.

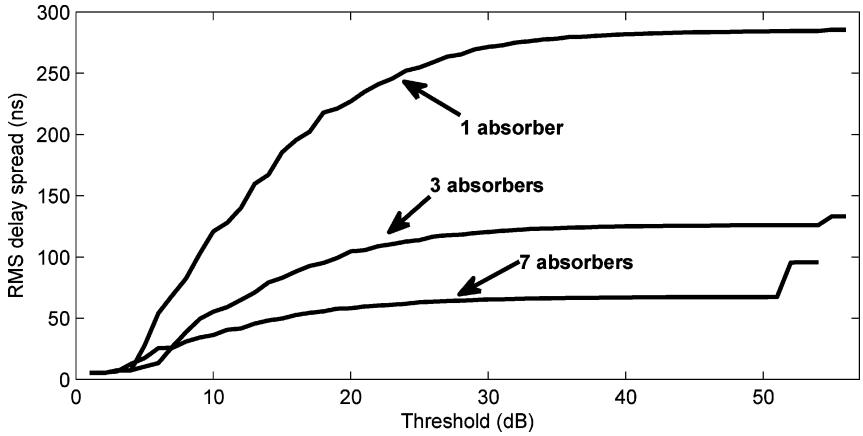

Fig. 3. RMS delay spread as function of the threshold for one, three, and seven absorbers.

as shown in [12]. For up to seven pieces of absorber blocks, our Q was still a factor of ten above $Q_{\rm thr}$. Hence, the field in this chamber using up to seven absorbers could still be considered as reasonably uniform, assuming sufficient averaging of the measured fields. In our experiments, one piece of absorber was a standard RF absorber block with nine cones in a 3×3 array. The taper length of each cone was 18 cm. In experiments discussed later in this paper, we used the individual cones that made up this absorber block in order to fine tune the loading of the chamber.

We calculated the RMS delay spread from the measured impulse response of the loaded chamber. To measure the impulse response of the reverberation chamber, we again used the two dual-ridge horn antennas and vector network analyzer measurement setup. The scattering parameter S_{21} was measured over a band of frequencies from 800 MHz to 12 GHz, and the inverse discrete Fourier transformation was applied. This was repeated for twenty different fixed paddle positions. The results were squared and averaged to obtain the PDP (as described in Section II). After that, we normalized the PDP to its maximum power.

The PDP results for zero, one, three, and seven pieces of absorber are shown in Fig. 2. The figure clearly shows the difference in decay for different levels of loading. For seven absorbers, the noise floor was reached only after1000 ns.

Use of measurements that have fallen below the noise floor of the instrumentation results in an artificially long RMS delay spread. However, it is necessary to use as long a time record as possible to obtain the best estimate of $\tau_{\rm rms}$. Thus, we bound the calculation to a certain threshold level. We define the threshold as the minimum signal level, below which the data are not utilized when calculating $\tau_{\rm rms}$. The threshold we used was relative to the maximum received-signal level in a given measurement.

In order to illustrate the dependence of the RMS delay spread on the threshold level, we calculated $\tau_{\rm rms}$ for different threshold values (see Fig. 3). This figure shows $\tau_{\rm rms}$ as a function of the absolute value of the threshold relative to the maximum value of the PDP. Depending on the number of absorbers, thresholds below -25 or -30 dB achieve the final value without falling below the noise floor, shown by the sudden increase in $\tau_{\rm rms}$ at around -50 dB. In order to compare $\tau_{\rm rms}$ for different loading, care needs to be taken in choosing a consistent threshold level for all measurements.

In general, the Q of the reverberation chamber is dependent on frequency. Because of this, use of a wide frequency range (such as the 800 MHz–12 GHz range used above in our impulse response calculation) to find the delay spread may skew results over the frequency band of interest. In order to analyze the behavior of the PDP and $\tau_{\rm rms}$ for a given frequency band, we

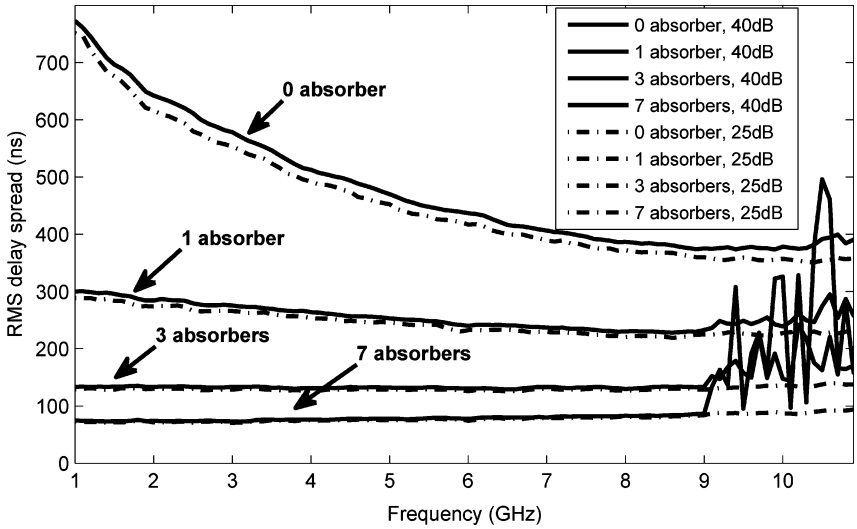

Fig. 4. RMS delay spread in the NIST reverberation chamber calculated over a 200-MHz bandwidth as a function of center frequency for different numbers of absorbers; -40 and -25 dB thresholds.

used a 200-MHz elliptic bandpass filter in postprocessing. This filter was applied to the measured S_{21} frequency-domain data, and the PDPs and τ_{rms} were calculated for different filter center frequencies.

The PDPs for a few center frequencies are shown in Fig. 4. Here, we swept the center frequency of the filter from 1 to 11 GHz and calculated τ_{rms} over a 200-MHz bandwidth. This was repeated for different numbers of absorbers. Results are shown for two threshold values: -25 and -40 dB. This figure shows that for zero absorber, τ_{rms} had a significant frequency dependence, while this frequency dependence diminished (that is, τ_{rms} did not change significantly) for increasing absorbers. The oscillations in the solid curve starting at 9 GHz for a higher number of absorbers can be explained by the choice of the threshold. For higher frequencies and a higher number of absorbers, the noise floor of the measurement system increased until it exceeded the -40-dB level at about 9 GHz, where it began to influence the results.

The reason for the strong frequency dependence for the no-absorber condition, and little-to-no frequency dependence for increasing numbers of absorbers can be explained by the following. For an ideal reverberation chamber, it can be shown that τ_{rms} is directly related to the chamber quality factor by the following [4]:

$$\tau_{\mathrm{rms}} = \frac{Q_{\mathrm{total}}}{2\pi f} \tag{8}$$

where f is the frequency and the total quality factor (assuming no aperture leakage) is given by [12]

$$Q_{\mathrm{total}}^{-1} = Q_{\mathrm{wall}}^{-1} + Q_{\mathrm{absorber}}^{-1} + Q_{\mathrm{antenna}}^{-1}. \tag{9}$$

Here, Q_{wall} is associated with the wall loss, Q_{absorber} is associated with absorber loss, and Q_{antenna} is associated with energy dissipated in the antenna. Using the expressions given in [12] for these various quality factors, τ_{rms} can be expressed as

$$\tau_{\mathrm{rms}} = \frac{1}{C_1\sqrt{f} + C_2\, N\, \sigma_{\mathrm{absorber}} + (C_3/f^2)}. \tag{10}$$

The first term in the denominator and its corresponding constant (C_1) are associated with the wall loss, the last term and its corresponding constant (C_3) are associated with the antenna. The second term and its constant (C_2) are associated with the loss due to the absorber. In the second term, $\sigma_{\mathrm{absorber}}$ is the absorption cross section of one absorber, and N is the number of absorbers in the chamber. The constants C_i are not given here but can be easily obtained from [12]. From this expression, we see that for very low frequencies, the third term dominates and is the major contribution to τ_{rms}. As the frequency increases, this term can be neglected, and if we assume no absorber, then $\tau_{\mathrm{rms}} \propto f^{-1/2}$. This is the type of variation seen in Fig. 4 for the no-absorber case. On the other hand, as the number of absorbers in the chamber increases, the second term in the expression dominates and $\tau_{\mathrm{rms}} \propto C$, that is, it becomes constant in frequency. This is the type of variation seen in Fig. 4 for increasing numbers of absorbers. The relationship between τ_{rms} and Q for nonideal environments is discussed in the next session.

With the information that we have now, it is possible to plot the RMS delay spread as a function of the number of absorbers. In this way, we can determine how many absorbers we need in order to achieve a certain delay spread. We have seen that the delay spread depends on frequency, therefore, we plot several curves for different center frequencies of the 200-MHz elliptical filter. Fig. 5 shows the measured RMS delay spread as a function of the number of absorbers for different center frequencies. As the numbers of absorbers increase, we see that τ_{rms} is independent of frequency, as (10) predicts.

Manufacturers of wireless systems who want to test their systems under certain multipath wireless conditions that are described by the RMS delay spread can simply create curves, such as in Fig. 5, to determine how many absorbers they need to test their devices for a certain delay spread and frequency *in their reverberation chamber*. As emphasized in the previous sentence, Fig. 5 is valid in only one specific reverberation chamber with a specific set of absorbers. In order to be more general and not

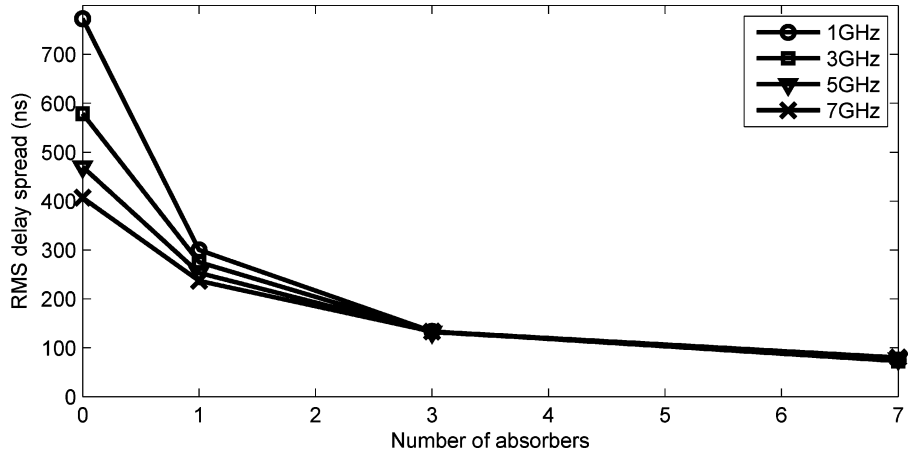

Fig. 5. Measured RMS delay spread as a function of the number of absorbers for different frequencies.

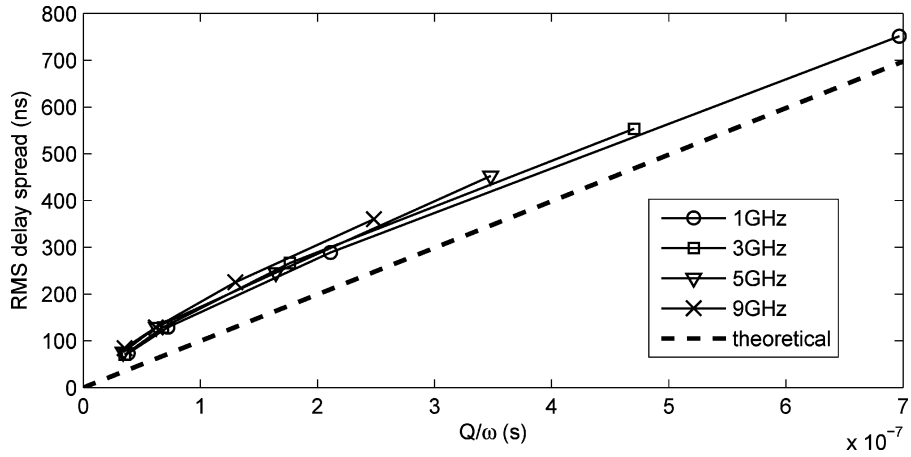

Fig. 6. Measured RMS delay spread as a function of the chamber time constant $\tau = Q/\omega$ for different frequencies.

bound to certain test setups, a more universal view is helpful. One such view will be described in the following.

A. RMS Delay Spread as a Function of the Chamber Time Constant

In theory, the energy in the chamber dissipates exponentially. The time constant $\tau = Q/\omega$ describes this effect [4]. Hence, the PDP should also have an exponential decay

$$\text{PDP}(t) = P_0\, e^{-t/\tau} = P_0\, e^{-\omega t/Q} \tag{11}$$

where P_0 is the maximum power.

In [34], Van't Hof derived an equation for the RMS delay spread as a function of $\tau = Q/\omega$. In this equation, a threshold α (in linear units) is considered

$$\tau_{\text{rms}} = \frac{Q}{\omega}\sqrt{\frac{(2\alpha\ln(\alpha) - 2\alpha + 2 - \alpha(\ln(\alpha))^2)}{(1-\alpha)} - \frac{(\alpha\ln(\alpha) - \alpha + 1)^2}{(1-\alpha)^2}} \tag{12}$$

for an ideal PDP, $\alpha \to 0$ and $\tau_{\text{rms}} = Q/\omega$.

Fig. 6 shows the measured RMS delay spread and the theoretical RMS delay spread, as calculated by use of (12), as a function of Q/ω. Even though there is an offset between the theoretical and measured curves, the slopes of all curves match very well. Part of the offset could be accounted for by a small amount of direct energy that may be present in the chamber. The point is presently being investigated and will be the topic of a future publication. These results show that the RMS delay spread is proportional to the ratio Q/ω. Hence, this model can be used to predict the approximate RMS delay spread for a given value of Q and frequency.

IV. BER Measurements

In order to study the effectiveness of how well a wireless system can be characterized in static multipath environments as simulated in a reverberation chamber, we carried out BER tests of digitally modulated signals. The measurement setup for obtaining the BER is shown in Fig. 7. To generate the signal, we used a vector signal generator (VSG). Using this generator, we could create waveforms with different symbol rate modulation types, carrier frequencies, or amplitudes. The VSG sends a repetitive, deterministic waveform whose period is

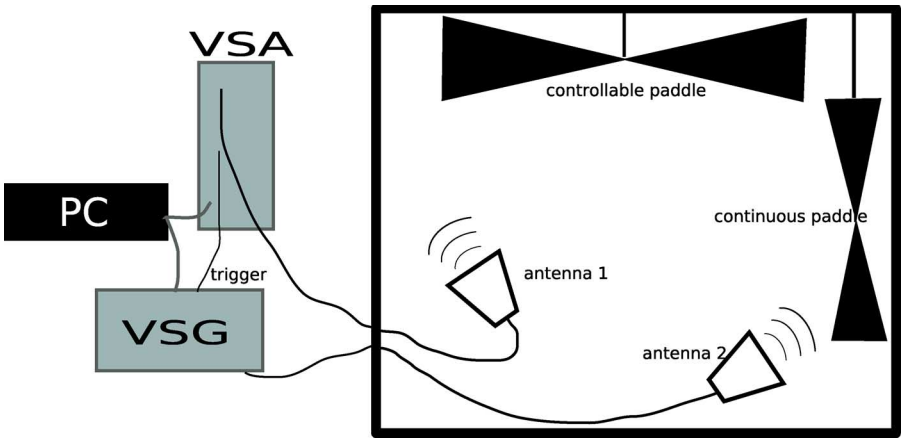

Fig. 7. BER measurement setup. VSG: vector signal generator; VSA: vector signal analyzer; and PC: a control and acquisition personal computer.

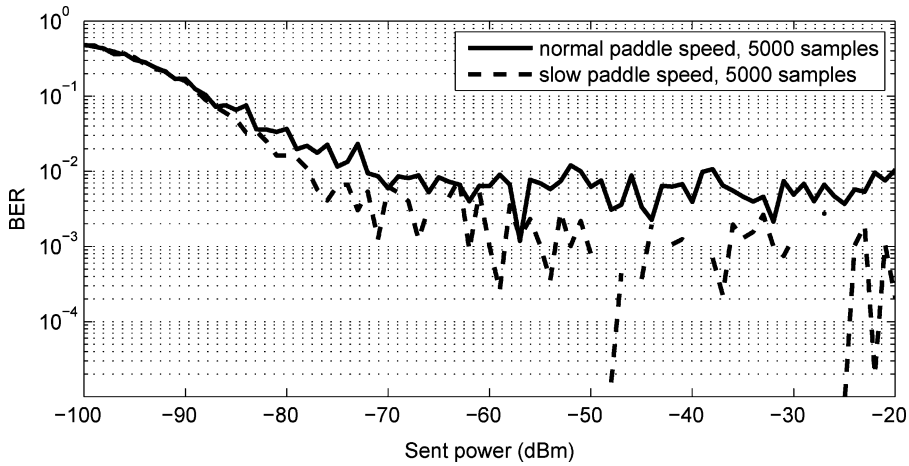

Fig. 8. BER for a 24.3 ksps BPSK signal, 5000 measured samples, fast and slow paddles.

determined by the number of bits sent. Since a deterministic bit pattern can influence results [29], it can cause results to differ slightly from theory, which is typically based on a random bit pattern.

In the following experiments, we used a bit sequence that was 1046 b long. In order to measure the BER, the received bits were compared with transmitted bits. These measurements were made several times (between 100 and 50 000 times), depending on the level of BER that we encountered. We used BPSK modulation with different symbol rates, as described in the following, and a carrier frequency of 700 MHz.

To receive the signal, we used a vector signal analyzer (VSA). The VSA can receive waveforms, demodulate them, and present the result as a sequence of ones and zeros. We triggered the VSA at the start of each bit pattern using the VSG. Again, we placed two dual-ridged horn antennas in the chamber pointing at different corners. Both paddles were turning continuously with a constant angular velocity.

In the graphs that follow, noise power was calculated in the same way we found the signal power, by integrating the received power across the measurement bandwidth. This bandwidth was held constant for both the signal and noise power measurements. It was set to around 80%–90% of the occupied bandwidth, as specified in many wireless standards.

We first performed a BER measurement with 5000 samples at a low symbol rate of 24.3 ks/s. 5 230 000 b = 1046 b·5000 were measured. The results are shown by the solid line in Fig. 8. The results are plotted as a function of transmitted power in order to see qualitative effects. It was necessary to transmit this large number of bits in order to collect meaningful BER results because, for channels having low BER values, we need to acquire a large number of bits before receiving an error. We see that the BER decreases for higher powers and stops decreasing at about 0.8% BER. This irreducible BER could have been caused by the limited correlation bandwidth in the chamber, fading, or by a combination of the two. The paddle was turning too slowly for Doppler shift to be a factor. Further studies to separately identify these effects are currently underway at NIST.

We next repeated the same measurement but decreased the velocities of both paddles. The results are shown by the dashed line in Fig. 8. We see that the BER for low SNR values, where measurement noise dominates, is similar for both curves. But for higher SNR values, the curves start to separate. The irreducible BER for the slower paddle speed is clearly below the results

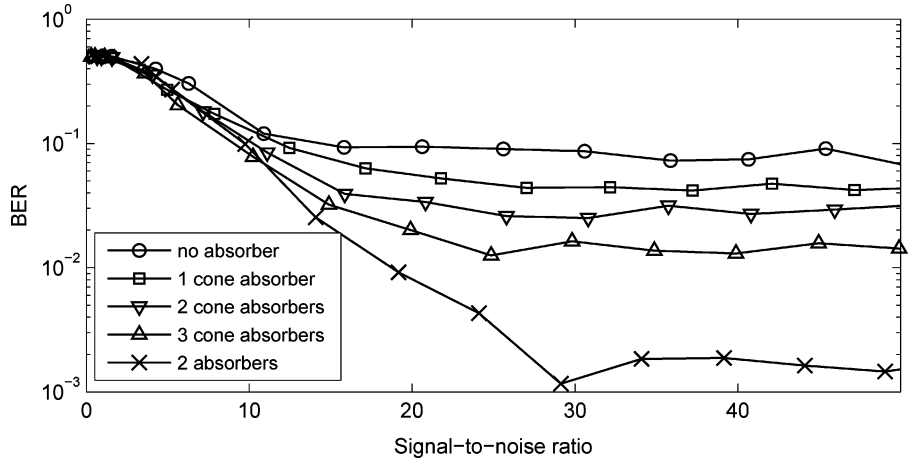

Fig. 9. BER for a measured 243 ksps BPSK signal for different amounts of absorber.

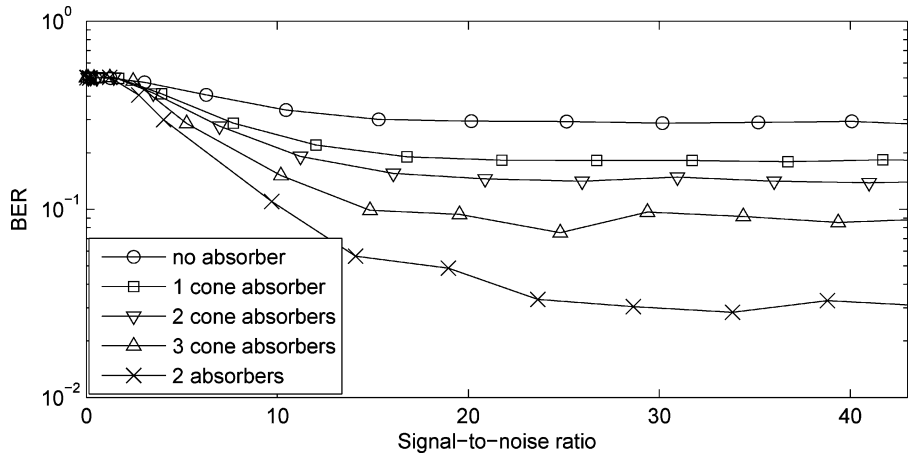

Fig. 10. BER for a measured 768 ksps BPSK signal for different amounts of absorber.

for the faster paddle speed, which is consistent with distortion caused by fading.

Our goal was to study the static multipath channel without the effects of fading so that we could compare to measurements made at a fixed location in a static multipath environment. Thus, the following measurements were performed with just one paddle operating at its lowest speed ($\approx 2.8 \times 10^{-3}$ r/s) in order to reduce fading and Doppler spread effects.

We next conducted measurements with higher symbol rates. According to Chuang [31], this would increase the irreducible BER since the ratio $(\tau_{\mathrm{rms}}/T)^2$ grows as the symbol period T becomes smaller. Figs. 9 and 10 show the BER for a modulated signal with 243 and 768 ksps, respectively.

In these figures, we first measured the BER for the no-absorber case and found that the irreducible BER was quite high (about 8%). When we put two absorbers inside, the BER dropped to a value where it was difficult to measure accurately. We then put one, two, and three cone absorbers inside, where each piece of absorber was one ninth of the size of a complete absorber. Recall the term absorber refers to a standard RF absorber block with nine cones in a 3×3 array. The taper length of each cone was 18 cm. It is interesting to note that the irreducible BER for just one individual cone absorber dropped by approximately a factor two, and for two whole absorbers by a factor of almost fifty.

The increased BER for slow (or stepped) paddle speeds and higher data-rate signals is due to the receiver's inability to lock onto a signal for paddle positions that create a very long duration fade within the passband of the measured signal. At slow paddle speeds, such a long duration fade maybe present as compared to a higher paddle speed. The paddle speed dependence is an interesting aspect of testing in reverberation chambers. This effect can also be utilized in order to obtain a repeatable, controllable deep-long-duration fading environment. This topic is being investigated further.

V. Comparisons to Real-World Environments

In order to illustrate the ability of the reverberation chamber to simulate a realistic multipath propagation environment, we compared the PDP measurements in the chamber for different loadings to two sets of PDP measurements: 1) a highly reflective industrial environment (an oil refinery in Denver, Colorado) and 2) a large 60-storied office building (in Denver, Colorado).

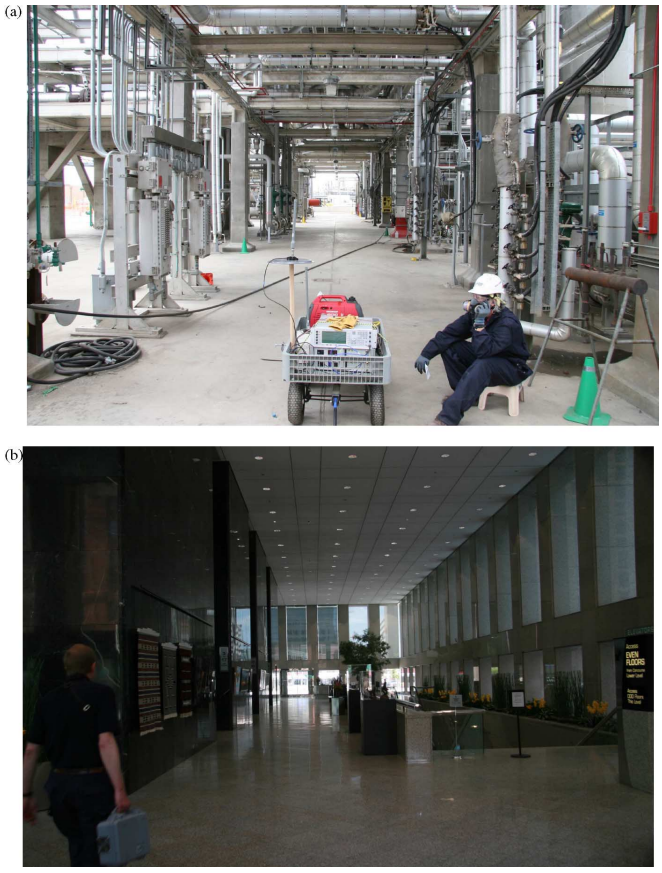

Fig. 11. (a) Oil refinery outside Denver, Colorado. (b) Sixty-storied office building in Denver, Colorado.

Attenuation and variability of radio wave signals associated with these two structures were studied in [30] and [35], respectively. The oil refinery consisted of several acres of piping and duct-work overhead and around the measurement setup, as shown in Fig. 11(a). The 60-storied office building was constructed from concrete and steel. The office building had large open areas on its lower floors, as shown in Fig. 11(b).

A comparison of the PDP measured in the reverberation chamber to the PDP measured in the oil refinery is plotted in Fig. 12. We used frequencies from 10 MHz to 1.8 GHz to calculate the PDP. We see a high level of multipath arising from this propagation environment, as shown by the long decay time of the PDP. Looking at the PDPs, we see that the PDP from the oil refinery environment best matches the reverberation chamber with three absorbers inside. The comparison of τ_{rms} values shown in the figure confirms this assumption.

The PDP from the reverberation chamber is again shown for various loading values and is compared in Fig. 13 to the PDP from the large open area in the 60-storied office building. We see a low level of multipath arising from this propagation environment, as shown by the relatively short decay time of the PDP. Looking at the PDPs, we see that the office building environment best matches the reverberation chamber with seven absorbers inside. The comparison of τ_{rms} values shown in the figure confirms this assumption.

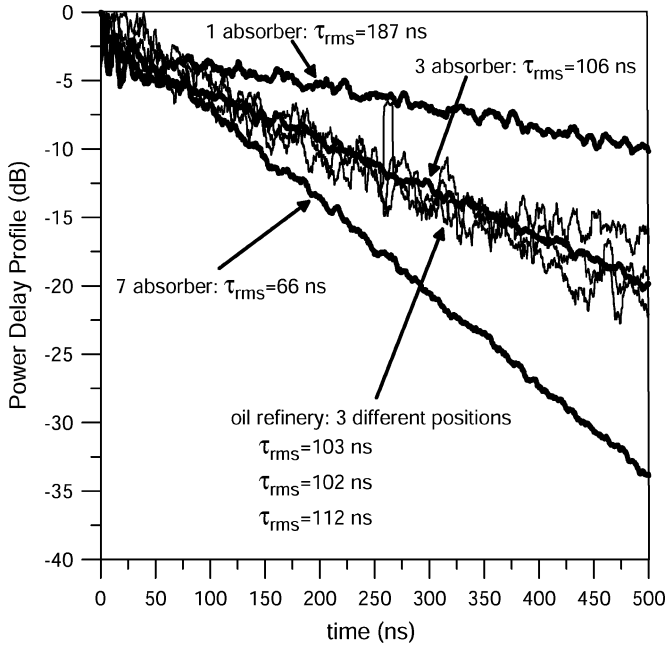

Fig. 12. Comparison of the PDP measured in the reverberation chamber for different amounts of absorber loading to the PDP measured in an oil refinery outside Denver, Colorado.

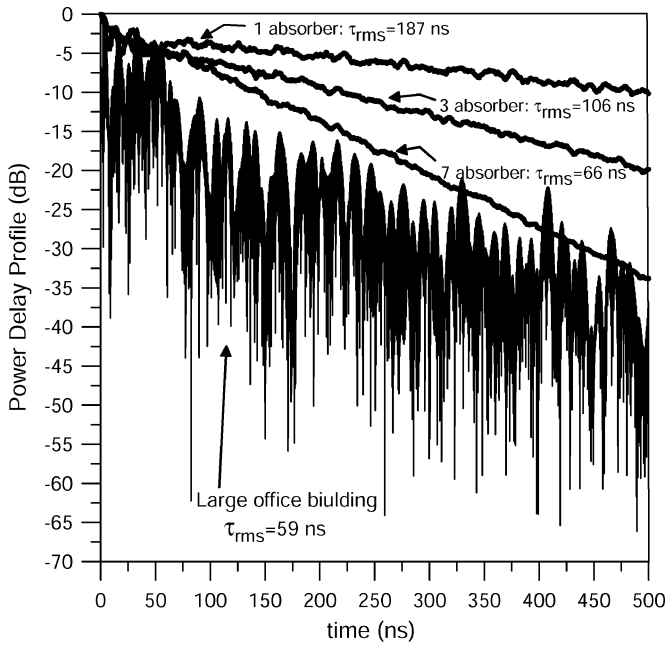

Fig. 13. Comparison of the PDP measured in the reverberation chamber for different amounts of absorber loading to the PDP measured in a 60-storied office building in Denver, Colorado.

These two comparisons show that the static multipath of two industrial/office environments may be simulated inside the chamber by adjusting the loading of the chamber. Simulating this and other industrial environments in the reverberation chamber can enable improved design and testing of wireless devices.

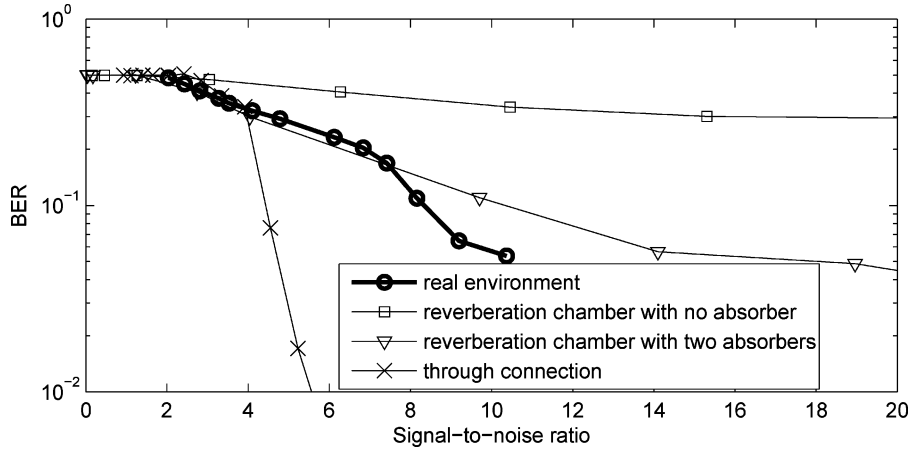

Fig. 14. Comparison of measured BER results from the reverberation chamber and from an office environment for a BPSK data rate of 768 ksps.

We also compared BER measurements obtained in the reverberation chamber for different loading values with a BER measurement in a real-world environment. The environment in this experiment was a NIST laboratory room with no shielded walls. The dimensions of the room were approximately 5 m (w) $\times$ 7 m (l) $\times$ 2.5 m (h). Three of the walls were cinder block material and the fourth was mostly windows. The floor was concrete, and piping and wiring were located above dropped ceiling tiles.

Data were collected using the VSA system described earlier. The transmitting antenna was a dual-ridge horn and the receiving antenna was a discone. The excitation was a BPSK digitally modulated signal with a data rate of 768 ksps. In order to obtain the BER measurement, we marked ten points on the floor spaced by distances of approximately 30 cm, and moved the receiving antenna from one point to another. For each position, the BER as function of excitation power was measured, and then the results were averaged over all antenna positions.

The results of the BER measurement in the real environment, together with the BER measurement in the reverberation chamber for different loading, values are shown in Fig. 14. This figure shows that the BER results were similar, particularly for higher values of BER. Because the BER values were quite low in the room environment, it was necessary to acquire a large number of data samples to obtain the BER using our VSA-based system. This significantly increased the measurement time. Even with this large number of samples, the agreement between the reverberation chamber measurements and the room measurements was not good. The simple VSA-based acquisition system presented in this paper works best for simulating higher multipath environments.

VI. Conclusion and Future Work

We demonstrated that it is possible to simulate various types of real-world wireless propagation environments inside a reverberation chamber by simulating both the PDP and the RMS delay spread. The reverberation chamber may be used as a reliable, repeatable test environment and, in contrast to an anechoic chamber or free space, a very efficient testing facility for these multipath wireless propagation measurements.

We showed experimentally that loading the chamber decreases the duration of the PDP, and hence, decreases the RMS delay spread value. The Q of the chamber was measured for different amounts of absorber material, and we showed that, for the number of absorbers used in our measurements, the field uniformity characteristics of the chamber were adequately maintained.

Data on RMS delay spread were presented as a function of frequency for different numbers of absorbers. By the use of the results presented here, it is feasible to predict the required number of absorbers for any given frequency in order to achieve the desired RMS delay spread for a given chamber.

BER measurements were also conducted inside the chamber. We showed that the BER, which is an indicator of the quality of a wireless communication channel, changed significantly when the chamber loading or the paddle speed was changed. Using the BER as an indicator, we showed that it is possible to simulate many desired wireless channel properties.

The results achieved in the reverberation chamber were compared to PDP measurements in an oil refinery and an office building and the results matched very well. BER measurements inside the chamber were also compared to those made in a low-multipath office environment. We showed that the results in the low-multipath environment were difficult to replicate using our simple receiver setup.

The reverberation chamber test methods presented here replicate a single, exponentially decaying PDP. This PDP adequately represents a number of wireless propagation environments, such as many outdoor-to-indoor channels and many indoor environments. However, other methods will be needed to replicate more complex environments, such as those involving clusters of exponentially distributed power delay profiles. This is currently a topic of research at NIST, for details see [26].

In future work, the difference between measured RMS delay spread and the RMS delay spread predicted with the chamber time constant should be examined. Experimental data are needed in order to verify the RMS delay spread prediction with chamber

Q. As well, further measurements are needed to verify effects of paddle speed, data rate, and transmission access scheme (such as global system for mobile or code division multiple access) on BER measured in the chamber. Finally, the paddle speed dependence is an interesting aspect of testing in reverberation chambers. This effect can also be utilized in order to obtain a repeatable, controllable deep-long-duration fading environment. This topic is being investigated further and will be the subject of a future publication.

ACKNOWLEDGMENT

The authors would like to thank D. Hill of NIST, Boulder, CO for his helpful suggestions and technical discussions on reverberation chambers, D. Camell and C. Grosvenor of NIST for providing the measured PDP industrial data, and S. Prather of AT&T, Seattle, WA, for his helpful suggestions on the BER measurements.

REFERENCES

[1] C. L. Holloway, D. A. Hill, J. M. Ladbury, P. Wilson, G. Koepke, and J. Coder, "On the use of reverberation chambers to simulate a controllable Rician radio environment for the testing of wireless devices," *IEEE Trans. Antennas Propag.*, vol. 54, no. 11, pp. 3167–3177, Nov. 2006.

[2] E. Genender, C. L. Holloway, K. A. Remley, J. Ladbury, G. Koepke, and H. Garbe, "Using reverberation chamber to simulate the power delay profile of a wireless environment," presented at the EMC Eur. 2008, Hamburg, Germany, Sep. 8–12.

[3] Electromagnetic compatibility (EMC) Part 4–21: Testing and Measurement Techniques Reverberation Chambers. IEC Standard 61000-4-21, 2003.

[4] D. A. Hill, "Electromagnetic theory of reverberation chambers," Nat. Inst. Stand. Technol., Boulder, CO, *NIST Tech. Note 1506*, 1998.

[5] D. A. Hill, "Plane wave integral representation for fields in reverberation chambers," *IEEE Trans. Electromagn. Compat.*, vol. 40, no. 3, pp. 209–217, Aug. 1998.

[6] P.-S. Kildal and C. Carlsson, "Detection of a polarization imbalance in reverberation chambers and how to remove it by polarization stirring when measuring antenna efficiencies," *Microw. Opt. Technol. Lett.*, vol. 32, no. 2, pp. 145–149, Jul. 20, 2002.

[7] B.-H. Liu, D. C. Chang, and M. T. Ma, "Eigenmodes and the composite quality factor of a reverberation chamber," Nat. Bureau Stand., Boulder, CO, *NBS Tech. Note 1066*, 1983.

[8] M. L. Crawford and G. H. Koepke, "Design, evaluation, and use of a reverberation chamber for performing electromagnetic susceptibility vulnerability measurements," Nat. Bureau Stand., Boulder, CO, *NBS Tech. Note 1092*, 1986.

[9] J. Ladbury, G. Koepke, and D. Camell, "Evaluation of the NASA Langley Research Center mode stirred chamber facility," Nat. Inst. Stand. Technol., Boulder, CO, *NIST Tech. Note 1508*, 1999.

[10] T. Nguyten, "RF loading effects of aircraft seats in an electromagnetic reverberating environment," in *Proc. 18th Digit. Avionics Syst. Conf.*, Oct. 24–29, 1999, vol. 2, pp. 10.B.5-1–10.B.5-7.

[11] D. M. Zhang, E. P. Li, T. K. D. Yeo, W. S. Chow, and J. Quek, "Influences of loading absorber on the performance of a reverberation chamber," in *Proc. IEEE Symp. Electromagn. Compat.*, Boston, MA, Aug. 18–22, 2003, pp. 279–281.

[12] D. A. Hill, M. T. Ma, A. Ondrejka, B. F. Riddle, M. Crawford, and R. Johnk, "Aperture excitation of electrically large, lossy cavities," *IEEE Trans. Electromagn. Compat.*, vol. 36, no. 3, pp. 169–178, Aug. 1994.

[13] D. A. Hill, J. Adams, M. Ma, A. Ondrejka, B. Riddle, M. Crawford, and R. Johnk, "Aperture excitation of electrically large, lossy cavities," Nat. Inst. Stand. Technol., Boulder, CO, *NIST Tech. Note 1361*, Sep. 1993.

[14] J. G. Kostas and B. Boverie, "Statistical model for a mode stirred chamber," *IEEE Trans. Electromagn. Compat.*, vol. 33, no. 4, pp. 366–370, Nov. 1991.

[15] C. L. Holloway, D. Hill, J. Ladbury, G. Koepke, and R. Garzia, "Shielding effectiveness measurements of materials in nested reverberation chambers," *IEEE Trans. Electromagn. Compat.*, vol. 45, no. 2, pp. 350–356, May 2003.

[16] C. L. Holloway, D. A. Hill, M. Sandroni, J. M. Ladbury, J. Coder, G. Koepke, A. C. Marvin, and Y. He, "Use of reverberation chambers to determine the shielding effectiveness of physically small, electrically large enclosures and cavities," *IEEE Trans. Electromagn. Compat.*, vol. 50, no. 4, pp. 770–782, Nov. 2008.

[17] N. Serafimov, P.-S. Kildal, and T. Bolin, "Comparison between radiation efficiencies of phone antennas and radiated power of mobile phones measured in anechoic chambers and reverberation chamber," in *Proc. 2002 IEEE Antennas Propag. Soc. Int. Symp.*, Jun. 2002, vol. 2, pp. 478–481.

[18] P.-S. Kildal, K. Rosengren, J. Byun, and J. Lee, "Definition of effective diversity gain and how to measure it in a reverberation chamber," *Microw. Opt. Technol. Lett.*, vol. 34, no. 1, pp. 56–59, Jul. 2002.

[19] P.-S. Kildal and K. Rosengren, "Electromagnetic analysis of effective and apparent diversity gain of two parallel dipoles," *IEEE Antennas Wireless Propag. Lett.*, vol. 2, pp. 9–13, 2003.

[20] K. Rosengren, P.-S. Kildal, C. Carlsson, and J. Carlsson, "Characterization of antennas for mobile and wireless terminals in reverberation chambers: Improved accuracy by platform stirring," *Microw. Opt. Technol. Lett.*, vol. 30, no. 20, pp. 391–397, Sep. 2001.

[21] K. Rosengren and P.-S. Kildal, "Radiation efficiency, correlation, diversity gain, and capacity of a six monopole antenna array for a MIMO system: Theory, simulation and measurement in reverberation chamber," *IEE Proc.-Microw. Antennas Propag.*, vol. 152, no. 1, pp. 7–16, Feb. 2005.

[22] M. Lienard and P. Degauque, "Simulation of dual array multipath channels using mode stirred reverberation chambers," *Electron. Lett.*, vol. 40, no. 10, pp. 578–579, May 2004.

[23] K. Rosengren and P.-S. Kildal, "Study of distributions of modes and plane waves in reverberation chambers for characterization of antennas in multipath environment," *Microw. Opt. Technol. Lett.*, vol. 30, no. 20, pp. 386–391, Sep. 2001.

[24] G. Ferrara, M. Migliaccio, and A. Sorrentino, "Characterization of GSM non-line-of-sight propagation channels generated in a reverberating chamber by using bit error rates," *IEEE Trans. Electromagn. Compat.*, vol. 49, no. 3, pp. 467–473, Aug. 2007.

[25] M. Otterskog and K. Madsen, "On creating a nonisotropic propagation environment inside a scattered field chamber," *Microw. Opt. Technol. Lett.*, vol. 43, no. 3, pp. 192–195, Nov. 2004.

[26] H. Fielitz, K. A. Remley, C. L. Holloway, Q. Zhang, Q. Wu, and D. W. Matolak, "Reverberation-chamber test environment for outdoor urban wireless propagation studies," *IEEE Antennas Wireless Propag. Lett.*, vol. 9, pp. 52–56, 2010.

[27] C. Orlenius, P.-S. Kildal, and G. Poilasne, "Measurements of total isotropic sensitivity and average fading sensitivity of CDMA phones in reverberation chamber," in *Proc. IEEE Antennas Propag. Soc. Int. Symp.*, Washington, DC, Jul. 3–8. 2005, vol. 1A, pp. 409–412.

[28] J. M. Ladbury, P. F. Wilson, G. H. Koepke, and T. Lammers, "Reverberation chamber: An evaluation for possible use as a RF exposure system for animal studies," in *Proc. Bio-Electromagn. Soc. (BEMS) 25th Annu. Meeting*, Maui, HI, Jun. 22–27, 2003, pp. 150–151.

[29] T. S. Rappaport, *Wireless Communications: Principles and Practice*. Upper Saddle River, NJ: Prentice-Hall, 1996.

[30] K. A. Remley, G. Koepke, C. L. Holloway, C. Grosvenor, D. Camell, J. Ladbury, D. Novotny, W. F. Young, M. D. McKinley, Y. Becquet, and J. Korsnes, "Measurements to support modulated-signal radio transmissions for the public-safety sector," Nat. Inst. Stand. Technol., Boulder, CO, *NIST Tech. Note 1546*, Oct. 2007.

[31] J. Chuang, "The effects of time delay spread on portable radio communications channels with digital modulation," *IEEE J. Sel. Areas Commun.*, vol. SAC-5, no. 5, pp. 879–889, Jun. 1987.

[32] S. R. Saunders and A. Aragon-Zavala, *Antennas and Propagation for Wireless Communication Systems*, 2nd ed. New York: Wiley, 2007, ISBN 978-0-470-84879-1.

[33] C. L. Holloway, D. A. Hill, J. M. Ladbury, and G. Koepke, "Requirements for an effective reverberation chamber: Unloaded or loaded," *IEEE Trans. Electromagn. Compat.*, vol. 48, no. 1, pp. 187–194, Feb. 2006.

[34] J. P. Van't Hof, "Modeling the dispersion and gain of RF wireless channels inside reverberant enclosures," Ph.D. thesis, Carnegie Mellon Univ., Pittsburgh, PA, Aug. 2005.

[35] W. F. Young, K. A. Remley, J. Ladbury, C. L. Holloway, C. Grosvenor, G. Koepke, D. Camell, S. Floris, W. Numan, and A. Garuti, "Measurements to support public-safety communications: Attenuation and variability of 750 MHz radio wave signals in three large building structures," Nat. Inst. Stand. Technol., Boulder, CO, *NIST Tech. Note 1552*, 2009.

Evgeni Genender (S'08) was born in Russia, in 1984. He received the Dipl.-Ing. (M.A.) degree in electrical engineering from Leibniz University of Hannover, Hannover, Germany, in 2009, where he is currently he is working toward the Ph.D. degree at the Institute of the Basics of Electrical Engineering and Measurement Science.

He was a Guest Researcher at the National Institute of Standards and Technology Boulder, CO, where he was involved in reverberation chambers. His research interests include investigation of IT networks and other large systems exposed (international) electromagnetic interference.

Christopher L. Holloway (S'86–M'92–SM'04–F'10) received the B.S. degree from The University of Tennessee, Chattanooga, in 1986, and the M.S. and Ph.D. degrees from the University of Colorado, Boulder, in 1988 and 1992, respectively, both in electrical engineering.

During 1992, he was a Research Scientist at Electro Magnetic Applications, Inc., Lakewood, CO, involved in theoretical analysis and finite-difference time-domain modeling of various electromagnetic problems. From the fall of 1992 to 1994, he was with the National Center for Atmospheric Research, Boulder, CO, where he was involved in wave propagation modeling, signal processing studies, and radar systems design. From 1994 to 2000, he was with the Institute for Telecommunication Sciences, U.S. Department of Commerce, Boulder, where he was involved in wave propagation studies. Since 2000, he has been with the National Institute of Standards and Technology, Boulder, where he is engaged in the research on electromagnetic theory. He is also on the Graduate Faculty at the University of Colorado, Boulder. His current research interests include electromagnetic field theory, wave propagation, guided wave structures, remote sensing, numerical methods, and electromagnetic compatibility (EMC)/electromagnetic interference (EMI) issues.

Dr. Holloway is a recipient of the 2008 IEEE EMC Society Richard R. Stoddart Award, the 2006 Department of Commerce Bronze Medal for his research on radio wave propagation, the 1999 Department of Commerce Silver Medal for his research in electromagnetic theory, and the 1998 Department of Commerce Bronze Medal for his research on printed circuit boards. He is currently the Co-Chair for Commission A of the International Union of Radio Science and is an Associate Editor for the IEEE TRANSACTIONS ON ELECTROMAGNETIC COMPATIBILITY. He was the chairman for the Technical Committee on Computational Electromagnetics (TC-9) of the IEEE EMC Society during 2000–2005, an IEEE Distinguished Lecturer for the EMC Society during 2004–2006, and is currently the Co-Chair for the Technical Committee on Nano-Technology and Advanced Materials (TC-11) of the IEEE EMC Society.

Kate A. Remley (S'92–M'99–SM'06) was born in Ann Arbor, MI. She received the Ph.D. degree in electrical and computer engineering from Oregon State University, Corvallis, in 1999.

From 1983 to 1992, she was a Broadcast Engineer in Eugene, OR. During 1989–1991, she was a Chief Engineer at an AM/FM broadcast station. She is currently at National Institute of Standards and Technology, Boulder, CO, where she joined Electromagnetics Division in 1999 as an Electronics Engineer. Her research interests include metrology for wireless systems, characterizing the link between nonlinear circuits and system performance, and developing methods for improved radio communications for the public-safety community.

Dr. Remley was the recipient of the Department of Commerce Bronze and Silver Medals and an Automatic RF Techniques Group Best Paper Award. She is currently the Editor-in-Chief of IEEE MICROWAVE MAGAZINE and Chair of the MTT-11 technical committee on microwave measurements.

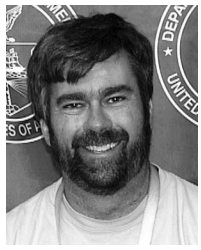

John M. Ladbury was born in Denver, CO, in 1965. He received the B.S.E.E. and M.S.E.E. degrees (specializing in signal processing) from the University of Colorado, Boulder, in 1987 and 1992, respectively.

Since 1987, he has been involved in Electromagnetic Compatibility (EMC) metrology and facilities at Radio Frequency Technology Division, National Institute of Standards and Technology, Boulder, CO. His research interests include reverberation chambers, with some investigations into other EMC-related topics such as time-domain measurements and probe calibrations.

Mr. Ladbury was involved in the revision of Radio Technical Commission for Aeronautics DO160D and is a member of the International Electrotechnical Commission joint task force on reverberation chambers. He has received three "Best Paper" Awards at IEEE International EMC symposia for the last six years.

Galen Koepke received the B.S.E.E. degree from the University of Nebraska, Lincoln, in 1973, and the M.S.E.E. degree from the University of Colorado, Boulder, in 1981.

He has contributed, over the years, to a wide range of electromagnetic issues such as measurements and research looking at emissions, immunity, electromagnetic shielding, probe development, antenna and probe calibrations, and generating standard electric and magnetic fields. Much of this work has focused on Transmission electron microscopy cell, anechoic chamber, open-area-test-site, and reverberation chamber measurement techniques along with a portion devoted to instrumentation software and probe development. He is currently a Project Leader for the Field Parameters and electromagnetic compatibility (EMC) Applications Program, Radio-Frequency Fields Group, National Institute of Standards and Technology (NIST), Boulder, CO. The goals of this program are to develop standards and measurement techniques for radiated electromagnetic fields and to apply statistical techniques to complex electromagnetic environments and measurement situations. A cornerstone of this program has been the work of NIST on complex cavities such as the reverberation chamber, aircraft compartments, etc.

Mr. Koepke is a National Association of Radio and Telecommunications Engineers (NARTE) certified EMC Engineer.

Heyno Garbe (F'06) received the Dipl.-Ing. (M.S.) and Dr.-Ing. (Ph.D.) degrees from the University of the Federal Armed Forces, Munich, Germany, in 1986 and 1978 respectively.

From 1986 to 1991, he was at Asea Brown Boveri Research Center, Baden, Switzerland, where he was involved in electromagnetic compatibility (EMC)-related topics. From 1991 to 1992, he was the Research Manager for EMC Baden Ltd., Switzerland. Since 1992, he has been at the Leibniz University of Hannover, Hannover, Germany, where he is a Professor in the Faculty of Electrical Engineering and Computer Science. He has delivered lectures on basic electrical engineering, measurement technology, and EMC, and also has developed an active research program related to electromagnetic field effect modeling, testing, and measurement as applied to EMC. He has authored or coauthored more than hundred articles published in books, journals, or conferences.

Dr. Garbe is a Fellow of electromagnetic pulse Summa Foundation. He is a member of URSI Com. E, VDE and other national and international professional organizations.